INSTITUTE OF PHYSICS PUBLISHING JOURNAL OF PHYSICS: CONDENSED MATTER

J. Phys.: Condens. Matter **16** (2004) 9069–9082 PII: S0953-8984(04)81020-8

Resonant Raman studies of compositional and size dispersion of $CdS_{1-x}Se_x$ nanocrystals in a glass matrix

Yu M Azhniuk[1], A G Milekhin[2], A V Gomonnai[1], V V Lopushansky[1], V O Yukhymchuk[3], S Schulze[4], E I Zenkevich[5] and D R T Zahn[4]

[1] Institute of Electron Physics, Ukranian National Academy of Sciences, Universytetska Street 21, Uzhhorod, 88000, Ukraine
[2] Institute of Semiconductor Physics, Novosibirsk, 630090, Russia
[3] Institute of Semiconductor Physics, Ukranian National Academy of Sciences, Prospect Nauky 45, Kyiv, 03028, Ukraine
[4] Institut für Physik, Technische Universität Chemnitz, Reichenhainer Straße 70, Chemnitz, 09107, Germany
[5] Institute of Molecular and Atomic Physics, National Academy of Sciences of Belarus, F. Skaryna Avenue 70, Minsk, 220072, Belarus

E-mail: azhn@ukrpost.net and azh@iep.uzhgorod.ua

Received 20 May 2004, in final form 24 September 2004
Published 26 November 2004
Online at stacks.iop.org/JPhysCM/16/9069
doi:10.1088/0953-8984/16/49/022

Abstract

Resonant Raman scattering spectra of glass-embedded $CdS_{1-x}Se_x$ nanocrystals are measured and complemented with TEM and optical absorption as well as photoluminescence data. The selectivity of the resonant Raman process not only for the size, but also for the composition of nanocrystals within the ensemble, is directly observed in the dependence of phonon band frequency, linewidth and shape on the excitation wavelength.

1. Introduction

Diffusion-limited growth from a supersaturated solution in a glass matrix is probably one of the most established ways to obtain semiconductor nanocrystals (quantum dots), and among these glass-embedded $CdS_{1-x}Se_x$ quantum dots undoubtedly belong to the most extensively studied [1, 2]. Besides the traditional use as optical cut-off filters, they have also found applications as non-linear optical devices ([1] and references therein), and, in particular, as active optical emitters in three-dimensional optical cavities called photonic dots and consisting of micrometre-sized glass spheres [3]. Shape, chemical composition, average size and size dispersion of nanocrystals are the main parameters determining their properties. Imaging by high-resolution transmission electron microscopy (HRTEM) provides direct evidence for an almost spherical shape of $CdS_{1-x}Se_x$ quantum dots grown in borosilicate glass and enables their size and size dispersion to be evaluated [4–6]. The average size can be also estimated from

small-angle x-ray scattering [5, 7] or optical absorption spectra [8, 9]. Chemical composition of semiconductor-doped glasses was in earlier papers determined by wet-chemical and x-ray fluorescence techniques. However, such analysis yields the amount of Cd, S and Se not only in the quantum dots but in the entire glass and cannot be used to determine the nanocrystal stoichiometry [10]. Determination of lattice parameters based on the analysis of x-ray diffraction data enables the average nanocrystal composition x to be estimated with the uncertainty of about 0.04 [10].

Raman spectroscopy is a fast and non-destructive technique for the estimation of the glass-embedded nanocrystal composition (from the optical phonon frequencies) [11] and size (from the frequencies of confinement-activated acoustic phonons) [5, 7, 12–14]. A number of detailed studies were devoted to specific broadening and asymmetry of the optical phonon bands in the Raman spectra of $CdS_{1-x}Se_x$ quantum dots, explained by the increasing role of surface phonons [15–20] as well as by confinement-induced scattering by phonons with non-zero wavevectors [16, 17, 19, 21–23]. Two more factors which can result in increasing phonon frequencies in the Raman spectra of $CdS_{1-x}Se_x$ nanocrystals are compressive strain arising from the glass matrix pressure [24, 25] and diffusion of zinc from the matrix to the nanocrystals in zinc-containing matrices [26–30].

$CdS_{1-x}Se_x$ quantum dots, grown in glass matrices, are characterized by fluctuation of both size and composition. The effect of disorder, induced by nanocrystal size fluctuations, on the Raman spectra was discussed in [31]. The size dependence of the Raman low-frequency scattering spectra from CdS nanocrystals was studied in [14] using different laser wavelengths for excitation to provide resonant scattering conditions. Resonant techniques are promising for the investigation of dilute systems like glass-embedded nanocrystals not only because they take advantage of the difference between the nanocrystals and the host matrix but also due to the sensitivity to the nanoparticle parameters. A detailed analysis of the resonant Raman scattering cross-section in CdSe quantum dots has shown that the main contribution to Raman scattering arises from the crystallites whose sizes favour incoming and outgoing resonance conditions [21]. It seems to be reasonable that in $CdS_{1-x}Se_x$ nanocrystals resonant Raman scattering should be sensitive not only to the size of nanoparticles, but also to their composition. However, as far as we know, no experimental observations of compositional dispersion of glass-embedded $CdS_{1-x}Se_x$ quantum dots by resonant Raman scattering have been reported so far.

Here we present the experimental results of resonant Raman scattering of $CdS_{1-x}Se_x$ quantum dots in a borosilicate glass matrix providing evidence for both size and compositional selectivity of the spectra recorded at different excitation conditions. Raman data are complemented with HRTEM images, optical absorption and photoluminescence spectra.

2. Experimental details

The investigated samples were $CdS_{1-x}Se_x$ nanocrystals, embedded in borosilicate glass matrix commercially available as Rubin cut-off filters of various modifications. The quantum dots were grown by the conventional technique of solid-state precipitation, similar to the method described in [4, 6, 10].

A set-up based on a LOMO DFS-24 double-grating monochromator with an FEU-136 phototube and Ar^+ laser operating at 488.0 and 514.5 nm was used for conventional resonant Raman scattering measurements. A Dilor XY 800 triple monochromator equipped with a CCD camera and a Kr^+ laser operating at 482.5 and 647.1 nm was employed for both conventional and micro-Raman measurements. The micro-Raman set-up enabled the exciting laser light to be focused to a 1 μm spot. The spectral resolution in all cases was within 2.5–3 cm^{-1}.

TEM preparation of the samples for microstructural investigations was performed following the procedure given in [32] including mechanical pre-thinning with a tripod grinding tool before being thinned to electron transparency by final ion etching in a Baltec RES 010 ion etching system. TEM measurements were performed using a Philips CM 20 FEG 200 keV transmission electron microscope equipped with a Gatan GIF imaging filter.

Optical absorption spectra were measured using a LOMO MDR-23 monochromator and an FEU-100 phototube with a resolution better than 2 nm.

Steady-state photoluminescence measurements were performed with a Shimadzu RF-5001PC spectrofluorimeter with appropriate spectral widths of the excitation (better than 5 nm) and emission (better than 20 nm) channels. Prior to carrying out steady-state photoluminescence experiments the spectrofluorimeter was calibrated for the spectral response of the detection channel against a set of fluorescence standards according to the procedure described in [33]. For samples with low (below 0.1–0.3) optical densities at the excitation wavelength the photoluminescence measurements were carried out in a transmittance geometry with an angle of $\sim 45^\circ$ between the excitation and detection directions. For samples with higher optical densities at the excitation wavelength, the measurements were performed in the reflection mode with an angle of $\sim 30^\circ$ between the excitation and detection directions in order to avoid or minimize the reabsorption influence on the blue side of photoluminescence spectra.

All measurements were performed at room temperature.

3. Results and discussion

First- and second-order Raman scattering spectra of the glass-embedded $CdS_{1-x}Se_x$ nanocrystals are shown in figure 1. This system of solid solutions is known to possess two-mode behaviour, i.e. the first-order Raman scattering spectrum of a mixed crystal contains both CdS- and CdSe-like phonons [34]. As seen from the figure, the observed divergence of the CdSe-like LO_1 and CdS-like LO_2 phonon bands is accompanied by the decrease of the LO_1 phonon intensity and the increase of the LO_2 phonon peak. Simultaneously in the second-order spectrum the weakening and downward shift of $2LO_1$ bands (from 410 to 389 cm^{-1}) is observed along with the increase of $LO_1 + LO_2$ (near 490 cm^{-1}, strong only for the samples with comparable content of S and Se) and (later) $2LO_2$ phonon bands. The latter also exhibits an upward shift from 569 to 594 cm^{-1}. This behaviour of Raman lines is due to the variation of the average composition of the quantum dots which can be estimated from the Raman spectra. For this purpose we plotted the difference of the CdS-like and CdSe-like LO phonon frequencies ω_2–ω_1 along the known reference plot based on the results of [11] complemented with those of other authors [20] (figure 2(a)). Note that plotting the LO phonon frequency difference significantly reduces the errors of x determination resulting from the glass matrix pressure as well as possible systematic instrumental errors. The applicability of such a method for the determination of $CdS_{1-x}Se_x$ nanocrystal composition in a broad compositional range was shown in [11] and its accuracy is estimated as 2–3%, being somewhat lower for the compositions close to CdSe and CdS due to the weakness of one of the phonon bands [11, 35]. As seen from figures 2(b) and (c), the experimental values of the CdS- and CdSe-like LO phonon frequencies in most cases are in agreement with the reference plot. Near $x = 0.5$ (OS-13N, OS-14N, and KS-10B samples) the observed frequencies are slightly (by 2–3 cm^{-1}) higher than the expected values. This can, in our opinion, be related to incorporation of zinc from the matrix into the nanocrystals during the diffusion-limited growth process. The zinc content in the nanocrystals can be estimated similarly to our earlier paper [30] and for the samples under investigation it does not exceed 5%.

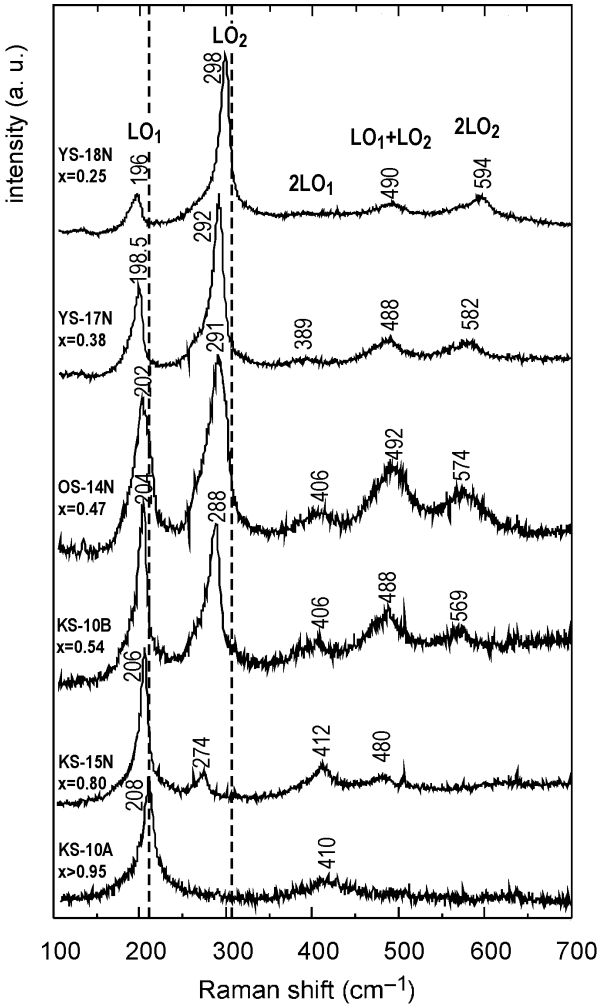

Figure 1. Micro-Raman spectra of $CdS_{1-x}Se_x$ nanocrystals embedded in borosilicate glass matrix, measured at room temperature with the excitation of the 482.5 nm laser line. The dashed lines corresponding to the LO phonon frequencies in CdSe and CdS are guides for the eyes. The indicated composition values were obtained from the Raman spectra and the plot of figure 2.

Optical absorption and photoluminescence spectra of glass-embedded $CdS_{1-x}Se_x$ nanocrystals, shown in figure 3, enabled us to obtain the energies of the electronic transitions in the nanocrystals. The maxima in the absorption spectra above the edge correspond to the confined electron–hole pair transitions in a spherical semiconductor quantum dot with a radius not exceeding the exciton Bohr radius. Using the assumption of the real part of the dielectric constant of the quantum dots as well as the oscillator strength per state being size independent, the effective-mass model gives the following expression for the energy position of the absorption maxima [36, 37]:

$$E_{(n_e,l_e),(n_h,l_h)} = E_b + \frac{\hbar^2}{2r^2}\left[\frac{\varphi^2_{n_e,l_e}}{m^*_e} + \frac{\varphi^2_{n_h,l_h}}{m^*_h}\right], \tag{1}$$

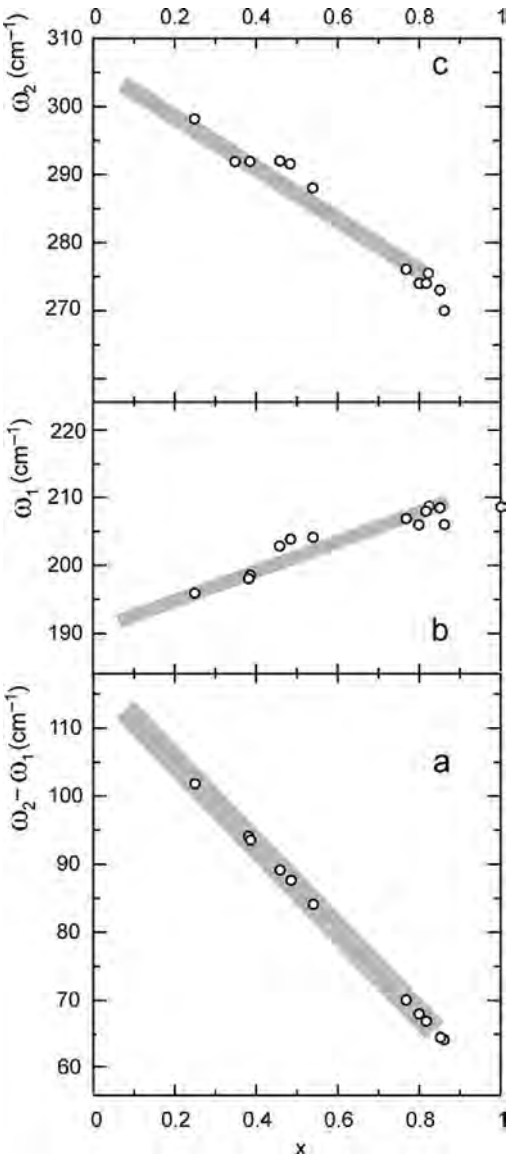

Figure 2. Compositional dependence of the difference of the observed CdS- and CdSe-like LO phonon frequencies (a) and the CdSe- and CdS-like frequencies themselves ((b) and (c), respectively) for the glass-embedded nanometric $CdS_{1-x}Se_x$ crystals. Broad grey lines indicate reference plots based on the data of [11, 20], the width corresponds to the generally considered x deviation of ± 0.03. Experimental data are denoted by open circles.

where E_b is the bulk energy gap, r is the quantum dot radius, $\varphi_{n,l}$ is the spherical Bessel function root for the corresponding quantum numbers, and m_e^* and m_h^* are the effective masses of electrons and holes, respectively. In $CdS_{1-x}Se_x$ the latter parameters can be determined by interpolation of the known values $m_e^* = 0.18\ m_0$ and $m_h^* = 0.53\ m_0$ for $x = 0$ [38] and $m_e^* = (0.11\text{–}0.13)\, m_0$ and $m_h^* = (0.44\text{–}0.63)\, m_0$ for $x = 1$ [21, 39], assuming a linear compositional variation in mixed crystals.

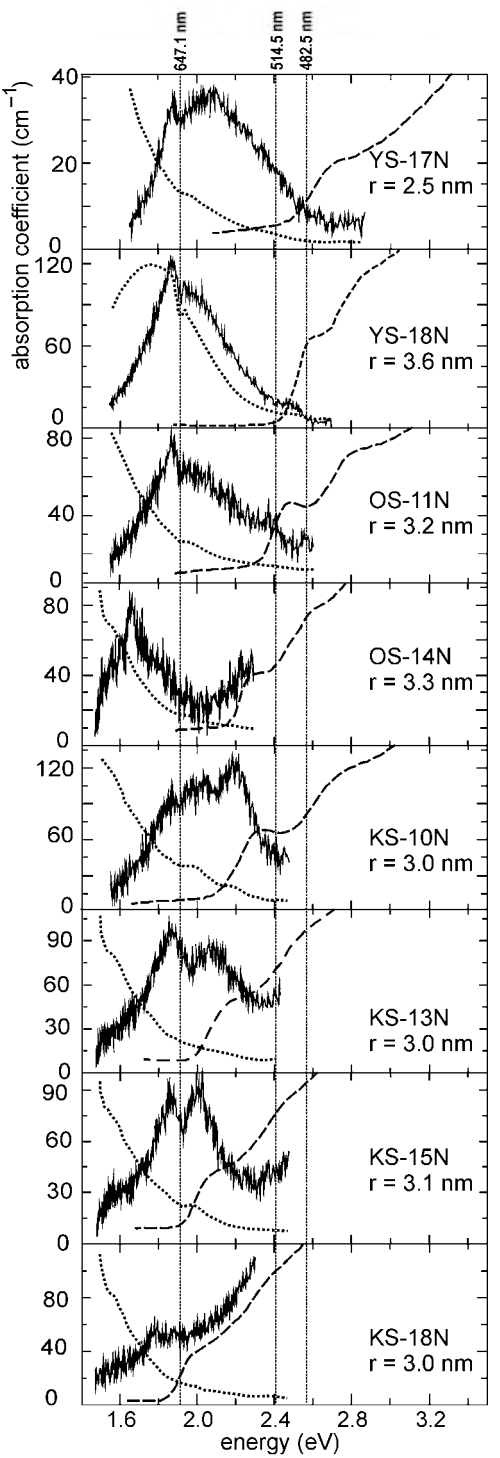

Figure 3. Optical absorption (dashed curves) and photoluminescence (solid curves—uncorrected, dotted curves—corrected for the spectrometer sensitivity) spectra of glass-embedded $CdS_{1-x}Se_x$ nanocrystals. Vertical short-dashed lines indicate the spectral positions of Raman excitation lines.

Table 1. Parameters of glass-embedded $CdS_{1-x}Se_x$ nanocrystals obtained from optical absorption and Raman spectra.

Sample label	Average radius (nm)	CdSe-like LO_1 phonon frequency (cm^{-1})	CdS-like LO_2 phonon frequency (cm^{-1})	Average composition, x
YS-17N	2.5	198.5	292	0.38
YS-18N	3.6	196	298	0.25
OS-11N	3.2	198[a]	292	0.38
OS-13N	3.3	203[a]	292[a]	0.46
OS-14N	3.3	203.5[a]	291[a]	0.48
KS-10A	3.2	208	—	1
KS-10B	3.3	204	288	0.54
KS-10N	3.0	206	276	0.77
KS-13A	3.9	208.5	273	0.85
KS-13N	3.1	206[a]	274[a]	0.80
KS-14N	3.1	206	274	0.80
KS-15N	3.1	206	274	0.80
KS-17N	3.0	207	274	0.82
KS-18N	3.0	206	270	0.86
KS-19N	3.1	205[a]	270[a]	0.84

[a] An asterisk indicates that for this sample a slight difference of the phonon peak frequency was observed for different excitation wavelengths. The value given in the table corresponds to the wavelength for which more nanocrystals were involved in the scattering process, i.e. to the case with higher Raman line halfwidth.

The compositions of the $CdS_{1-x}Se_x$ quantum dots, determined from Raman scattering, as well as their average radii, derived from the measured absorption spectra, are listed in table 1. One can see that the estimated radii are in good agreement with data obtained by HRTEM (see figure 4) which also clearly show the near-spherical shape of the nanocrystals in the host matrix. Note that obtaining HRTEM images was strongly encumbered by strong charging of the sample and waggling of the pattern. The good agreement of HRTEM and absorption results shows, similarly to [8], the absorption-based method to be quite reliable for the estimation of the average size of II–VI semiconductor nanocrystals dispersed in a dielectric matrix.

The appearance of the observed photoluminescence spectra is rather typical for the glass-embedded $CdS_{1-x}Se_x$ quantum dots. In almost all cases two broad peaks are observed, the position of one of them (1.85 eV) being practically the same for all samples, independent of their absorption edge position, nanocrystal average size and composition. This luminescence band is usually associated with deep trap states in the nanocrystals like surface defects, size-substituted impurities or vacancies [10, 40, 41]. In samples with sulfur-rich nanocrystals another broad mid-gap luminescence maximum is observed at 2.0–2.2 eV (see figure 3, solid curves). For the samples with higher selenium content the observed higher-energy maximum in the photoluminescence spectra corresponds to the near-edge emission, also observed in [40, 41]. However, one should mention that the earlier papers reported the luminescence spectrum without references to correction for the spectrometric set-up sensitivity profile. Meanwhile, such correction, if performed, indicates an intense emission band centred in the near-infrared spectral range and smearing of the maxima in the range of 1.8–2.4 eV (dotted curves in figure 3). This can result, in particular, from the increase of the correction uncertainty for the low-energy part of the luminescence spectrum due to the ratio of a low signal to a low sensitivity factor which is related to the lack of suitable photodetectors for this range. The detailed discussion of the photoluminescence spectra of $CdS_{1-x}Se_x$ quantum dots will be given in a forthcoming paper. However, it should be noted that in some cases luminescence, the intensity of which is

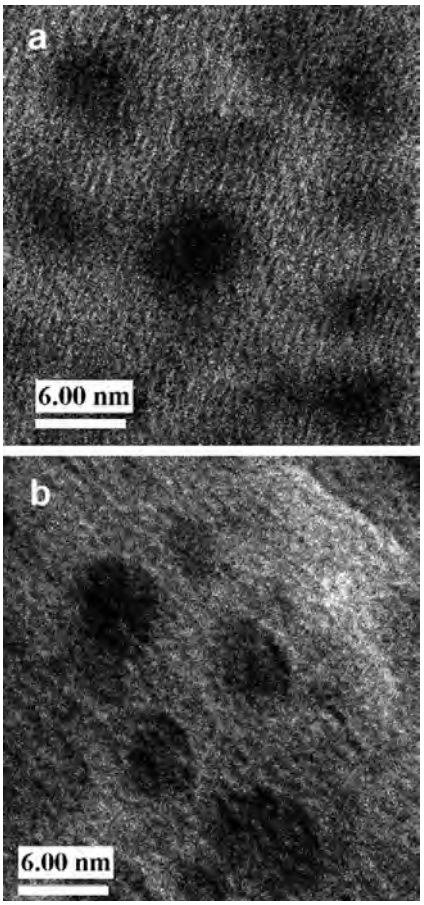

Figure 4. HRTEM images of YS-17N (a) and KS-13A (b) samples of $CdS_{1-x}Se_x$ nanocrystals in a borosilicate glass matrix.

known to exhibit resonance behaviour [40], strongly encumbered Raman signal detection at certain excitation wavelengths.

In most cases the shape of the observed LO phonon bands in the Raman spectra of the glass-embedded quantum dots is typically asymmetric with a more pronounced low-frequency side (figure 1). This fact is usually related to several effects. The nanocrystal size results in an increasing contribution of scattering by surface phonon modes below the corresponding LO phonon frequencies [15–18, 42]. Raman scattering by nonzero-wavevector phonons arising from the relaxation of selection rules due to phonon confinement leads to the downward shift of the phonon bands accompanied by asymmetric broadening [43, 44]. On the other hand, the effect of compressive strain in the nanocrystals due to the host matrix pressure estimated to be about 0.5 GPa [37–39] can result in an LO phonon frequency increase by about 1% [27]. This correlates with the experimentally observed values of pressure-induced LO phonon frequency shift in borosilicate glass-embedded $CdS_{1-x}Se_x$ quantum dots of 5 cm^{-1} GPa^{-1} [40, 41]. Finally, the Raman lineshape can be considerably affected by compositional disorder resulting from the spread of the $CdS_{1-x}Se_x$ nanocrystal composition within the ensemble.

The detailed analysis of the effects on the Raman lineshape of $CdS_{1-x}Se_x$ quantum dots embedded in borosilicate glass reveals that for the nanocrystal size range under investigation

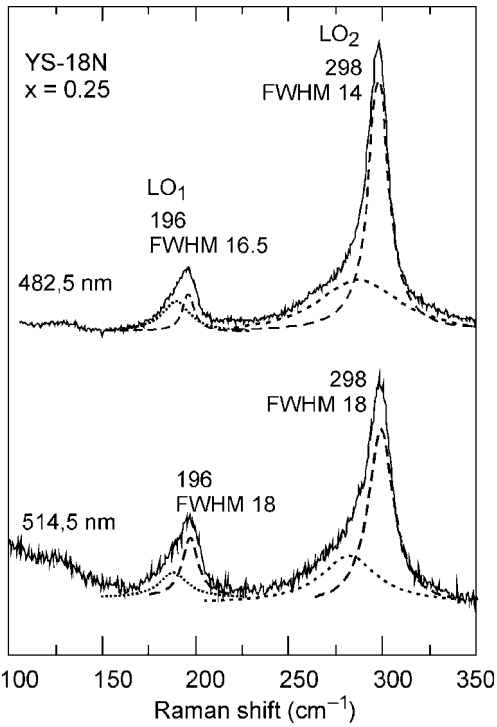

Figure 5. First-order Raman spectrum of the YS-18N sample with $CdS_{0.75}Se_{0.25}$ nanocrystals embedded in borosilicate glass matrix measured at different excitation wavelengths (solid curve) and simulation of the observed phonon maxima by superimposing relevant 'bulk' LO (dashed curves) and surface (dotted curves) phonons.

the predominant contribution to the Raman line asymmetry arises from surface phonons [20]. The performed calculations show that the confinement-related nonzero-wavevector phonon contribution to the Raman spectrum becomes significant for considerably smaller $CdS_{1-x}Se_x$ nanocrystals. Hence, each observed first-order Raman spectrum can be simulated by superimposing two relatively narrow 'bulk' CdSe-like LO_1 and CdS-like LO_2 phonon peaks and two broader surface bands at frequencies somewhat below those of the 'bulk' phonons. This is important for the analysis of the band halfwidths.

In some cases the Raman spectra showed a dependence on the excitation wavelength. For instance, for the sample labelled YS-18N ($x = 0.25$) the LO_1 and LO_2 bands observed at the excitation with 482.5 nm laser light were somewhat narrower (FWHM 16.5 and 14 cm^{-1}, respectively) than in the case of 514.5 nm laser light excitation (18 cm^{-1} each). This is even more noticeable for the purely 'bulk' LO_1 and LO_2 phonons: 8 and 11 cm^{-1}, respectively, for $\lambda_{exc} = 482.5$ nm, and 11 and 13 cm^{-1} for $\lambda_{exc} = 514.5$ nm (figure 5). It can be seen from figure 3 that in the case of $\lambda_{exc} = 482.5$ nm the excitation energy coincides with the lowest-energy transition for the YS-18N sample, providing incoming resonance conditions. In this case the main contribution to the Raman spectrum comes from quantum dots with radii in the range $|R_e - R| < \delta R$ where R_e denotes the radius for which the resonance is achieved. The δR value can be estimated from the equation

$$\Gamma_\mu = \frac{\partial E_\mu(R)}{\partial R}\delta R \tag{2}$$

where E_μ is the energy of the excitonic state participating in the resonance and Γ_μ is the excitonic state lifetime broadening [21]. The calculations performed for glass-embedded CdSe quantum dots ($R_e = 2$ nm) with a reasonable value of $\Gamma_\mu = 5$ meV gave $\delta R = 0.02$ nm [21]. In our case the dependence of Raman linewidths on the excitation wavelength results from the resonant Raman selectivity to the nanocrystal size and at $\lambda_{exc} = 482.5$ nm only the nanocrystals matching the resonance conditions contribute to the scattering intensity. However, in our opinion, the range of the radii of such nanocrystals is much broader than $\delta R = 0.02$ nm. Otherwise, since the beam was focused on a ~ 1 μm spot (micro-Raman scattering) and, as follows from HRTEM data (figure 4), the nanocrystal size dispersion is about 20%, the scattering intensity would be much lower and strongly variable over the sample surface area, which is obviously not the case. For the average nanocrystal radius 3.6 nm (YS-18N sample) the $\partial E_\mu(R)/\partial R$ value is smaller; besides, at room temperature a higher Γ_μ value should be assumed. Both these factors result in higher δR. Moreover, in our case of $CdS_{1-x}Se_x$ nanocrystalline solid solution, the resonant Raman process is also composition sensitive and resonance conditions are fulfilled not only for the nanocrystal size range δR, but also for the compositional interval δx:

$$\Gamma_\mu = \frac{\partial E_\mu(R,x)}{\partial R}\delta R + f(x)\frac{\partial E_\mu(R,x)}{\partial x}\delta x \tag{3}$$

where $f(x)$ is the nanocrystal composition distribution function over the ensemble. Therefore, in the case of the YS-18N sample δR and δx values can hardly be estimated separately.

An even more pronounced dependence of the Raman linewidth on the excitation wavelength is observed for selenium-rich nanocrystals. For example, as seen in figure 6, for the sample KS-15N ($x = 0.80$, $R = 3.1$ nm) in the case of $\lambda_{exc} = 647.1$ nm the LO_1 phonon peak at 206 cm^{-1} is quite narrow (5.5 cm^{-1}) and practically symmetric while for $\lambda_{exc} = 428.5$ and 514.5 nm it is much broader (12.5–14.5 cm^{-1}) and asymmetric due to the surface phonon contribution. 428.5 and 514.5 nm excitation light falls rather deep into the absorption range while $\lambda_{exc} = 647.1$ nm corresponds to a luminescence maximum of the KS-15N sample (figure 3). This latter case seems to exhibit distinct nanocrystal size and/or composition selectivity which follows not only from the LO_1 phonon peak narrowing, but also from its much lower intensity (cf signal-to-noise ratio for $\lambda_{exc} = 647.1$ and 482.5 nm in figure 6) at the same acquisition time.

Moreover, the surface phonon band appears to be quite sensitive to the Raman excitation wavelength. While being observed as a pronounced asymmetry on the lower frequency side of the LO_1 phonon peak at $\lambda_{exc} = 482.5$ and 514.5 nm, it totally vanishes at $\lambda_{exc} = 647.1$ nm. The surface phonon frequency is considered to be independent of the nanocrystal size [17] and rather weakly dependent on the composition of the $CdS_{1-x}Se_x$ nanocrystalline solid solution [15, 17, 20], although experimentally in CdSe quantum dots a size-dependent surface phonon mode was reported [18]. One can suppose that the resonance enhancement of the LO_1 mode is probably much larger than that of the surface phonon. A similar behaviour when approaching the direct bandgap is reported for resonant Raman studies of GaP quantum dots [45]. However, in InAs/AlGaAs quantum dot structures resonant enhancement of interface modes is observed [46], hence generally a similar behaviour could be expected for surface modes. An alternative explanation for the observed Raman line narrowing and vanishing of the asymmetry at $\lambda_{exc} = 647.1$ nm can be the fact that in this case resonant excitation conditions correspond to the nanocrystals of larger size for which the surface-to-volume ratio is smaller, hence the surface mode scattering intensity is smaller as well [47, 48].

As seen from figure 7, a similar LO_1 phonon band narrowing and lack of asymmetry at $\lambda_{exc} = 647.1$ nm with respect to the case of higher-energy Raman excitation are observed for the KS-18N sample ($x = 0.86$, $R = 3.0$ nm). For this material $\lambda_{exc} = 647.1$ nm

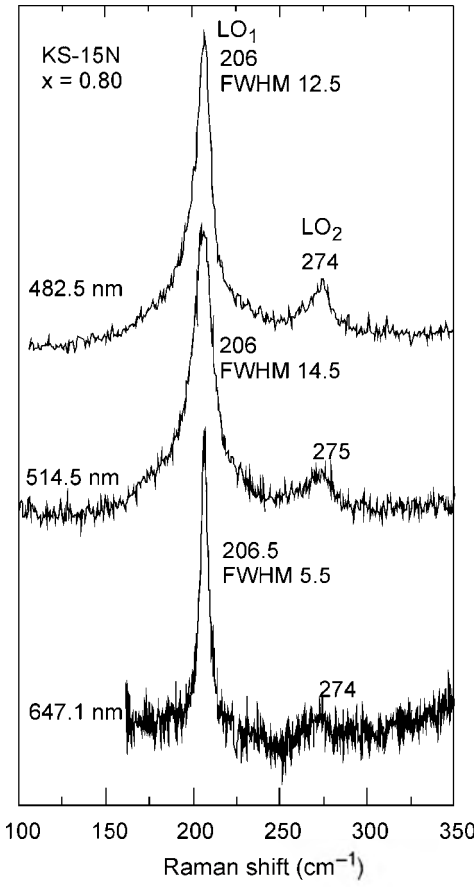

Figure 6. First-order Raman spectrum of the KS-15N sample with $CdS_{0.20}Se_{0.80}$ nanocrystals embedded in borosilicate glass matrix measured at different excitation wavelengths. Phonon peak frequencies and widths (FWHM) are indicated in cm^{-1}.

corresponds to the incoming resonance with the lowest energy transition. Besides, here one can also observe the peak frequency of the LO_1 phonon to shift to 209 cm^{-1} with respect to 206 cm^{-1} for $\lambda_{exc} = 482.5$ and 514.5 nm. Simultaneously, the position of the much weaker LO_2 phonon maximum is also dependent on the excitation wavelength (270–272 and 274 cm^{-1}, respectively). The LO_1 phonon peak narrowing (from 11 to 7.5 cm^{-1}) and frequency shift under the excitation wavelength variation observed for both Stokes and anti-Stokes scattering unambiguously indicate the Raman scattering selectivity to the composition of $CdS_{1-x}Se_x$ nanocrystals due to the incoming Raman resonance. Moreover, as seen from the figure, the frequency positions of the $2LO_1$ phonon peak in the second-order spectrum are also dependent on the excitation wavelength: 412 cm^{-1} ($\lambda_{exc} = 482.5$ and 514.5 nm) and 418 cm^{-1} ($\lambda_{exc} = 647.1$ nm) (see figure 7). This difference (6 cm^{-1}) is twice as high as the one observed for the LO_1 phonon position and considerably above the experimental resolution.

The qualitative observation of the resonant Raman selectivity for nanocrystals of certain compositional interval δx within the nanoparticle ensemble in the glass matrix is beyond any doubt. As to the quantitative estimations of the δx value as well as the evaluation of the compositional dispersion of the glass-embedded nanocrystals, they can be based on the

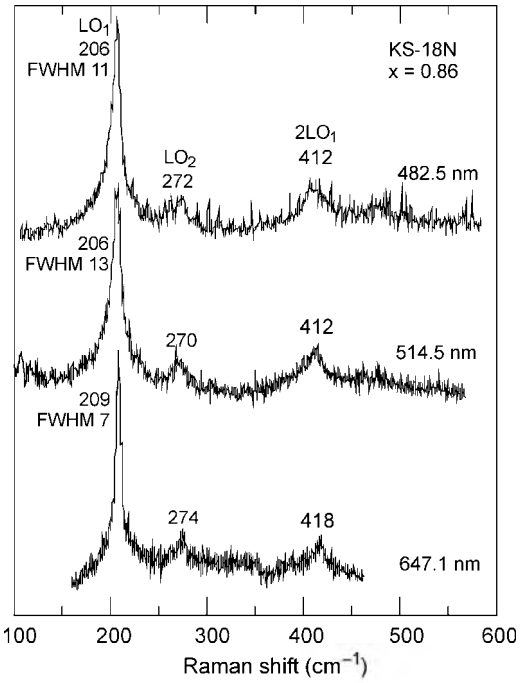

Figure 7. First- and partly second-order Raman spectrum of KS-18N sample with $CdS_{0.14}Se_{0.86}$ nanocrystals embedded in borosilicate glass matrix measured at different excitation wavelengths. Phonon peak frequencies and widths (FWHM) are indicated in cm^{-1}.

difference between the CdSe-like LO_1 and CdS-like LO_2 phonon frequencies $\omega_2 - \omega_1$ as the measure of the quantum dot composition. The case of Raman excitation deep in the absorption range ($\lambda_{exc} = 482.5$ and 514.5 nm) when the whole ensemble of the quantum dots contributes to the Raman process yields a value of $\omega_2 - \omega_1 = 64$ cm^{-1} corresponding to the average composition $x = 0.86$ (see figure 2). In the case of incoming resonance with the lowest energy transition ($\lambda_{exc} = 647.1$ nm) $\omega_2 - \omega_1 = 66$ cm^{-1} corresponds to the value of $x = 0.83$ for the nanocrystals contributing to the resonant Raman spectrum. The difference between these compositions shows that the compositional dispersion δx for the $CdS_{1-x}Se_x$ nanoparticle ensemble in the glass matrix is at least 0.03 and therefore comparable to the accuracy in the determination of the $CdS_{1-x}Se_x$ nanocrystal composition by Raman spectroscopy. In fact, however, the determination of the nanocrystal composition merely on the basis of the LO phonon frequency difference in this case is encumbered by the low content of one component resulting in an increasing uncertainty of the corresponding LO peak position determination due to its weak intensity. In such a case the LO_1 to LO_2 phonon intensity ratio is often taken as a complementary measure of x [11, 30]. For the KS-18N sample this intensity ratio corresponds to $x = 0.78$ ($\lambda_{exc} = 482.5$ nm), $x = 0.83$ ($\lambda_{exc} = 514.5$ nm), and $x = 0.91$ ($\lambda_{exc} = 647.1$ nm). Besides, since at $\lambda_{exc} = 647.1$ nm both maxima shift towards higher frequencies with respect to the average values for the ensemble (see figure 7), one may conclude that it is not only a pure change of x which is responsible for the nanocrystal composition variation within the nanoparticle ensemble.

Variation of x results in the change of the corresponding phonon frequency difference (convergence or divergence of the LO_1 and LO_2 phonon bands) while, as known from [26–30], simultaneous shift of both maxima indicates the presence of zinc in the nanocrystals

due to its diffusion from the zinc-containing matrix in the course of the nanocrystal ripening. Hence, similarly to the spread in selenium content x, there can exist a spread in zinc content y in the nanocrystals within the ensemble. Since the presence of zinc results not only in the upward shift of both LO_1 and LO_2 phonon frequencies, but also in a bandgap broadening, this can lead to the matching of the Zn-containing nanocrystals to the resonance conditions for $\lambda_{exc} = 647.1$ nm and to the dependence of LO_1 and LO_2 phonons on the excitation wavelength observed in figure 7. Hence, one may conclude that some of the nanocrystals in the ensemble can contain a noticeable amount of zinc, which in the case of the KS-18N sample is estimated from the Raman spectra as about 5% (for the nanocrystals matching the conditions of Raman resonance with $\lambda_{exc} = 647.1$ nm). The actual values of x and y spread in the glass-embedded nanocrystal ensemble can be somewhat higher than those determined from the resonant Raman scattering since for a more exact determination a tunable-wavelength laser is required as well as, probably, a more extensive set of the samples with different nanocrystal sizes and compositions. However, in our opinion, even the qualitative observation of resonant Raman selectivity to the composition of individual nanocrystals within the glass-embedded $CdS_{1-x}Se_x$ nanoparticle ensemble as well as the rough estimations of the compositional spread are important since, as far as we know, no other techniques are capable of providing the corresponding data.

4. Conclusions

The analysis of resonant Raman scattering spectra of $CdS_{1-x}Se_x$ nanocrystals embedded in borosilicate glass in a broad compositional range, complemented with TEM, optical absorption and photoluminescence data, has revealed CdSe- and CdS-like LO phonon frequency and linewidth dependence on the Raman excitation wavelength. It is shown that in the case of incoming or outgoing resonance with an electronic transition the main contribution in the observed Raman spectra comes from nanocrystals in the ensemble the size and composition of which match the resonance conditions. As follows from the observed phonon lineshape, the contribution of surface phonons which do not exhibit such resonant behaviour is much smaller in this case. The estimations of $CdS_{1-x}Se_x$ compositional spread in the sample show that it is caused not only by the variation of selenium content within at least 3%, but also by partial (below 5%) substitution of Cd by Zn in some of the nanocrystals of the ensemble.

The obtained results contribute to the discussion on the applicability of Raman scattering for the determination of composition of dilute nanocrystals embedded in dielectric media. It can be concluded that the accuracy of the Raman technique within $\Delta x = 0.02$–0.03 [11, 35] is somewhat overestimated. In fact it is determined not only by the CdS- and CdSe-like LO phonon frequency difference, but also affected by several other effects, sensitive to the Raman excitation conditions. However, Raman spectroscopy still remains the most efficient and accurate technique to determine the composition of mixed semiconductor nanocrystals dispersed in a dielectric matrix.

Acknowledgment

The first author is grateful to Deutscher Akademischer Austauschdienst for the opportunity granted to carry out the research at the Institute of Physics, Chemnitz University of Technology (reference A/03/20352).

References

[1] Woggon U and Gaponenko S V 1995 *Phys. Status Solidi* b **185** 285
[2] Woggon U 1997 *Optical Properties of Semiconducting Quantum Dots* (Berlin: Springer)

[3] Jia R, Jiang D S, Tan P H and Sun B Q 2001 *Appl. Phys. Lett.* **79** 153
[4] Liu L-C and Risbud S H 1990 *J. Appl. Phys.* **68** 28
[5] Champagnon B, Andrianasolo B, Ramos A, Gandais M, Allais M and Benoit J-P 1993 *J. Appl. Phys.* **73** 2775
[6] Ekimov A 1996 *J. Lumin.* **70** 1
[7] Irmer G, Monecke J, Verma P, Goerigk D and Herms M 2000 *J. Appl. Phys.* **88** 1873
[8] Kulish N R, Kunets V P and Lisitsa M P 1997 *Fiz. Tverd. Tela* **39** 1865
Kulish N R, Kunets V P and Lisitsa M P 1997 *Phys. Solid State* **39** 1667 (Engl. Transl.)
[9] Gomonnai A V, Azhniuk Yu M, Lopushansky V V, Megela I G, Turok I I, Kranjčec M and Yukhymchuk V O 2002 *Phys. Rev.* B **65** 245327
[10] Borrelli N F, Hall D, Holland H and Smith D 1987 *J. Appl. Phys.* **61** 5399
[11] Tu A and Persans P D 1991 *Appl. Phys. Lett.* **58** 1506
[12] Lipinska-Kalita K E, Mariotto G and Zanghellini E 1995 *Phil. Mag.* B **71** 547
[13] Roy A and Sood A K 1996 *Solid State Commun.* **97** 97
[14] Saviot L, Champagnon B, Duval E and Ekimov A I 1998 *Phys. Rev.* B **57** 341
[15] Mlayah A, Brugman A M, Carles R, Renucci J B, Valakh M Ya and Pogorelov A V 1994 *Solid State Commun.* **90** 567
[16] Roy A and Sood A K 1996 *Phys. Rev.* B **53** 12127
[17] Ingale A and Rustagi K C 1998 *Phys. Rev.* B **58** 7197
[18] Hwang Y N, Park S H and Kim D 1999 *Phys. Rev.* B **59** 7285
[19] Verma P, Gupta L, Abbi S C and Jain K P 2000 *J. Appl. Phys.* **88** 4109
[20] Gomonnai A V, Azhniuk Yu M, Yukhymchuk V O, Kranjčec M and Lopushansky V V 2003 *Phys. Status Solidi* b **239** 490
[21] Trallero-Giner C, Debernardi A, Cardona M, Menendez-Proupin E and Ekimov A I 1998 *Phys. Rev.* B **57** 4664
[22] Sirenko A A, Belitsky V I, Ruf T, Cardona M, Ekimov A I and Trallero-Giner C 1998 *Phys. Rev.* B **58** 2077
[23] Vasilevskiy M I, Rolo A G and Gomes M J M 1997 *Solid State Commun.* **104** 381
[24] Scamarcio G, Lugara M and Manno D 1992 *Phys. Rev.* B **45** 13792
[25] Hwang Y N, Shin S, Park H L, Park S H, Kim U, Jeong H S, Shin E J and Kim D 1996 *Phys. Rev.* B **54** 15120
[26] Yükselici H, Persans P D and Hayes T M 1995 *Phys. Rev.* B **52** 11763
[27] Rajalakshmi M, Sakuntala T and Arora A K 1997 *J. Phys.: Condens. Matter* **9** 9745
[28] Persans P D, Lurio L B, Pant J, Lian G D and Hayes T M 2001 *Phys. Rev.* B **63** 115320
[29] Yükselici M H 2001 *J. Phys.: Condens. Matter* **13** 6123
[30] Azhniuk Yu M, Milekhin A G, Gomonnai A V, Lopushansky V V, Turok I I, Yukhymchuk V O and Zahn D R T 2004 *Phys. Status Solidi* a **201** 1578
[31] Vasilevskiy M I, Rolo A G, Gomes M J M, Vikhorova O V and Ricolleau C 2001 *J. Phys.: Condens. Matter* **13** 3491
[32] Benedict J B, Anderson R and Klepens S J 1992 *Mater. Res. Soc. Symp. Proc.* **254** 121
[33] Gardecki J A and Maroncelli M 1998 *Appl. Spectrosc.* **52** 1700
[34] Beserman R 1977 *Solid State Commun.* **23** 323
[35] Miyoshi T, Nakatsuka T and Matsuo N 1995 *Japan. J. Appl. Phys.* **34** 1835
[36] Efros Al L and Efros A L 1982 *Fiz. Tekh. Poluprovodn.* **16** 1209
Efros Al L and Efros A L 1982 *Sov. Phys.—Semicond.* **16** 772 (Engl. Transl.)
[37] Gaponenko S V 1998 *Optical Properties of Semiconductor Nanocrystals* (Cambridge: Cambridge University Press)
[38] Lippens P E and Lannoo M 1989 *Phys. Rev.* B **39** 10935
[39] Cohen R and Sturge M D 1982 *Phys. Rev.* B **25** 3828
[40] Ivanda M, Bischof T, Materny A and Kiefer W 1997 *J. Appl. Phys.* **82** 3116
[41] Verma P, Irmer G and Monecke J 2000 *J. Phys.: Condens. Matter* **12** 1097
[42] Hayashi S and Yamamoto K 1986 *Superlatt. Microstruct.* **2** 581
[43] Campbell I H and Fauchet P M 1986 *Solid State Commun.* **58** 739
[44] Fauchet P M and Campbell I H 1988 *Crit. Rev. Solid State Mater. Sci.* **14** S79
[45] Efros Al L, Ekimov A I, Kozlowski F, Petrova-Koch V, Schimidbaur H and Shumilov S 1991 *Solid State Commun.* **78** 853
[46] Milekhin A G, Toropov A I, Bakarov A K, Tenne D A, Zanelatto G, Galzerani J C, Schulze S and Zahn D R T 2004 *Phys. Rev.* B **70** 085313
[47] Milekhin A G, Sveshnikova L L, Repinsky S M, Gutakovsky A K, Friedrich M and Zahn D R T 2002 *Thin Solid Films* **422** 200
[48] Nanda K K and Sahu S N 1997 *Appl. Surf. Sci.* **119** 50